

---

# InfoGAN-CR: Disentangling Generative Adversarial Networks with Contrastive Regularizers

---

Zinan Lin\*      Kiran K. Thekumparampil†      Giulia Fanti‡      Sewoong Oh§

## Abstract

Training disentangled representations with generative adversarial networks (GANs) remains challenging, with leading implementations failing to achieve comparable performance to Variational Autoencoder (VAE)-based methods. After  $\beta$ -VAE and FactorVAE discovered that regularizing the total correlation of the latent vectors promotes disentanglement, numerous VAE-based methods emerged. Such a discovery has yet to be made for GANs, and reported disentanglement scores of GAN-based methods are significantly inferior to VAE-based methods on benchmark datasets. To this end, we propose a novel regularizer that achieves higher disentanglement scores than state-of-the-art VAE- and GAN-based approaches. The proposed *contrastive regularizer* is inspired by a natural notion of disentanglement: *latent traversal*. Latent traversal refers to generating images by varying one latent code while fixing the rest. We turn this intuition into a regularizer by adding a discriminator that detects how the latent codes are coupled together, in paired examples. Numerical experiments show that this approach improves upon competing state-of-the-art approaches on benchmark datasets.

## 1 Introduction

Learning low-dimensional, informative data representations can critically enhance the data’s utility. The notion of *disentangled* representations in particular was theoretically proposed in [5, 36, 17] for diverse applications including supervised and reinforcement learning. These ideas were later empirically validated in [20] for learning hierarchical visual concepts and in [18] for improving the robustness of reinforcement learning algorithms. A disentangled generative model takes a number of interpretable latent factors as input, with each factor controlling one aspect of the generated data. For example, in facial images, disentangled latent factors might control variations in eyes, noses, and hair.

Most approaches for disentangling latent factors (or *codes*) are based on the following natural intuition. We say a generative model has a better disentanglement if changing one latent code (while fixing other latent codes) makes a *noticeable* and *distinct* change in the generated sample. Noticeable changes are desired as we want the latent codes to capture important characteristics of the image. Distinct changes are desired as we want each latent code to represent an aspect of the samples different from other latent codes. As such, a successful disentanglement is typically evaluated by traversing the latent space as in Figure 1: by fixing all latent codes except one, varying that code systematically, and visualizing the resulting changes. Figure 1 illustrates how the latent codes  $\{c_1, \dots, c_5\}$  of a generator have been successfully trained to capture noticeable and distinct properties of the images.

Recent approaches have focused on adding carefully chosen regularizers to promote disentanglement, building upon the two popular deep generative models: Variational AutoEncoders (VAE) [24]

---

\*Carnegie Mellon University, zinanl@andrew.cmu.edu

†University of Illinois at Urbana-Champaign, thekump2@illinois.edu

‡Carnegie Mellon University, gfanti@andrew.cmu.edu

§University of Washington, sewoong@cs.washington.edu

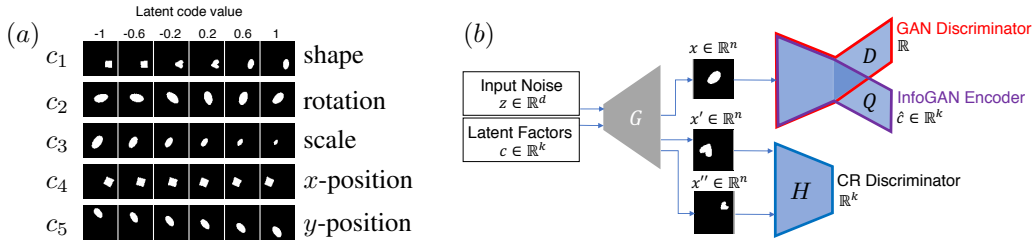


Figure 1: (a) Each row shows how the image changes when traversing a single latent code while fixing the rest, as captured by the proposed InfoGAN-CR trained on the dSprites dataset (details in Section 4). The latent codes capture desired disentangled properties, {shape, rotation, scale,  $x$ -pos,  $y$ -pos}, of the image. (b) Like InfoGAN, InfoGAN-CR includes a GAN discriminator  $D$  and an encoder  $Q$ , which share all convolutional layers and have separate fully-connected final layers. In addition, the CR discriminator  $H$  takes as input a pair of images  $x'$  and  $x''$  that are generated by sharing one fixed latent factor  $c'_i = c''_i$  for a randomly chosen  $i \in [k]$ , and randomly drawing the rest. The discriminator is trained to correctly identify  $i$ , the index of the fixed factor.

and Generative Adversarial Networks (GAN) [15]. However, fundamental difference in these two architectures led to the design of different regularizers. In a standard VAE training, an encoder finds a compact representation of real data, and a decoder is used to reconstruct the original image from the latent representation. To achieve disentanglement, a popular approach is to add an extra regularizer to promote “*uncorrelatedness*” by making each latent code distinct, as in  $\beta$ -VAE [17].

In a standard GAN, a neural network generator is trained to map a randomly-drawn noise vector to the domain of the real data. A discriminator is introduced to encourage the generated sample distribution to be close to the real data. Disentangled GANs add a secondary input of latent codes, which are meant to control the underlying factors. The loss function then adds an extra regularizer to promote “*informativeness*”, as proposed in InfoGAN [8]. However, InfoGAN has been quantitatively reported to be significantly inferior to its VAE-based counterparts, which led to slow progress on GAN-based disentangled representation learning.

**Related work.** Learning a disentangled representation was first demonstrated in the *semisupervised setting*, where additional annotated data is available. This consists of examples from desired isolated latent factor traversals [22, 25, 33, 29]. However, as manual data annotation is costly, *unsupervised methods* for disentangling are desired. Early approaches to unsupervised disentangling imposed uncorrelatedness by making it difficult to predict one representational unit from the rest [38], disentangling higher order moments [10], using factor analysis [41], and applying group representations [9]. Breakthroughs in making these ideas scalable were achieved by  $\beta$ -VAE [17] for VAE-based methods, and InfoGAN [8] for GAN-based ones. Rapid progress in improving disentanglement was driven mainly by VAE-based methods, in a series of papers including [23, 28, 7, 29, 4, 13, 14, 35, 11, 2, 1]. Quantitative comparisons in these papers suggest that InfoGAN cannot learn good disentangled representations. This has led to a misconception that GAN-based methods are inherently poor at learning disentangled representations.

**Main contributions.** We first disprove the common misconception that InfoGAN is inferior by training an InfoGAN model to achieve a disentanglement comparable to the best VAE-based method (FactorVAE [23]). This is achieved by stabilizing the training using spectral normalization and two time-scale update rules, thus suggesting that the previously-reported poor performance of InfoGAN is due to training choices, not fundamental differences. We next design an appropriate regularizer to improve upon it. We propose a novel regularizer from the first principles of disentanglement, which we call a *contrastive regularizer* (CR). We show that the new architecture InfoGAN-CR achieves a significant gain over competing state-of-the-art approaches on benchmark datasets.

**Overview of InfoGAN-CR.** Our proposed regularizer is inspired by the idea that disentanglement should be measured via changes in the images when traversing the latent space. This is a popular interpretation of disentanglement, as evidenced by the widely-adopted visual evaluation of disentanglement (e.g. Figure 1). To measure such changes, we naturally pair two (or more) samples drawn from one of multiple appropriately-designed joint distributions by *coupling* the two random latent vectors. We introduce a new discriminator that performs multiway hypothesis testing on which joint distribution was used to create the paired examples. The loss of this discriminator provides an

additional regularization, which we call Contrastive Regularization (CR). Building upon InfoGAN’s architecture (see Section 2 for details), we add contrastive regularization and refer to the resulting architecture as InfoGAN-CR, illustrated in Figure 1 (right).

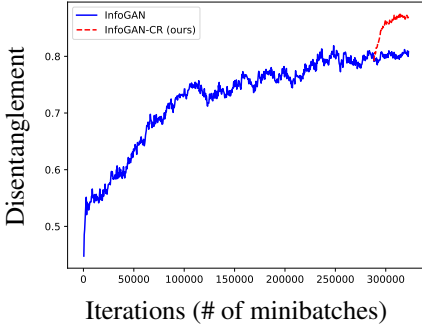


Figure 2: After 288,000 iterations, we continue training InfoGAN with/without the proposed contrastive regularizer. The jump at the split point illustrates the gain due to the proposed regularizer. The curves are averaged over 10 instances on the same data.

(288,000 iterations), and keep training with an added CR-regularizer (red curve), precisely defined in Eq. (6). All other hyperparameters are identical. We measure disentanglement using the popular metric of [23] and defined in Section 4. The jump at epoch 28 suggests that contrastive regularization significantly enhances disentanglement, on top of what was achieved by InfoGAN regularizer alone.

## 2 Improving InfoGAN via stabilizing training

In this section, we give a brief overview of InfoGAN, introduced in [8]. Specifically, we highlight the design and training choices that have led to the misconception that InfoGAN cannot achieve disentanglement comparable to competing approaches. We disprove this misconception empirically by achieving a performance comparable to the best reported disentanglement scores (Table 1), by applying recently introduced techniques for stabilizing GAN training. We also derive in Remark 1 an implicit bias term that arises in practical InfoGAN implementations.

**Background on GAN.** Generative Adversarial Networks (GANs) are a breakthrough method for training generative models proposed in [15]. A deep neural network generative model maps a latent code  $z \in \mathbb{R}^d$  to a desired distribution of the samples  $x = G(z)$ .  $z$  is typically drawn from a Gaussian distribution with identity covariance. To train the neural network  $G$ , no likelihood is available for ML training. GANs instead update the weights of a generator  $G$  and discriminator  $D$  using alternative gradient updates on the following *adversarial loss*:

$$\min_G \max_D \mathcal{L}_{\text{Adv}}(D, G). \quad (1)$$

The discriminator provides an approximate measure of how different the current generator distribution is from the distribution of the real data. For example, a common choice is  $\mathcal{L}_{\text{Adv}}(D, G) = \mathbb{E}_{x \sim P_{\text{real}}}[\log(D(x))] + \mathbb{E}_{P_G}[\log(1 - D(x))]$ , which provides an approximation of the Jensen-Shannon divergence between the real data distribution  $P_{\text{data}}$  and the current generator distribution  $P_G$ .

**Background on InfoGAN.** In order to achieve disentanglement, InfoGAN proposes a regularizer based on mutual information. As the goal is not to disentangle all latent codes, but rather to disentangle a subset, InfoGAN [8] proposed to first split the latent codes into two parts: the disentangled code vector  $c \in \mathbb{R}^k$  and the remaining code vector  $z \in \mathbb{R}^d$  that provides additional randomness. InfoGAN then uses the GAN loss with regularization to encourage informative latent codes  $c$ :

$$\min_G \max_D \mathcal{L}_{\text{Adv}}(G, D) - \lambda I(c; G(c, z)), \quad (2)$$

Concretely, the input to the generator is partitioned into two parts: a latent vector  $c \in \mathbb{R}^k$  that learns the disentangled representation and input noise  $z \in \mathbb{R}^d$  that provides additional randomness. We generate a pair of test samples  $x'$  and  $x''$  from a pair of  $(c', z')$  and  $(c'', z'')$ . We design a set of joint distributions over  $c'$  and  $c''$ , and treat them as multiple hypotheses on how the pair  $(x', x'')$  is generated. This paired example is now fed into a discriminator  $H$ , which tries to detect which hypothesized coupling was used. Both the generator  $G$  and the CR discriminator  $H$  try to make this hypothesis testing successful. We design the hypotheses to encourage each latent code to make changes that are easy to detect: noticeable and distinct, hence encouraging disentanglement. Contrastive regularization is discussed in detail in Section 3.

Figure 2 is an experiment focused on illustrating how the proposed contrastive regularizer enhances disentanglement beyond vanilla InfoGAN. The blue curve shows the performance when we train a vanilla InfoGAN on dSprites dataset for 28 epochs (322,560 iterations) total. To show the effect of the proposed CR regularizer, we take the model we just trained with InfoGAN at 25 epochs

where  $I(c; G(c, z))$  denotes the mutual information between the latent code  $c$  and the sample  $G(c, z)$  generated from that latent code, and  $\lambda$  is a positive scalar coefficient. Notice that encouraging informativeness alone does not necessarily imply good disentanglement; a fully entangled representation can achieve infinite mutual information  $I(c; G(c, z))$ . Despite this, InfoGAN achieves reasonable performance in practice. Its empirical performance follows from implementation choices that promote stability and alter the InfoGAN objective, which we discuss next.

**Practical implementation of InfoGAN loss and the resulting implicit bias.** Let  $P_{c,x}$  denote the joint distribution of the latent code  $c$  and the generated image  $x = G(c, z)$ . Two structural assumptions are enforced in [8] to make the maximization of  $I(c; x)$  tractable. First, to make optimization of the mutual information tractable, all practical implementations of InfoGAN replace  $I(c; x)$  with a variational lower bound  $\max_{Q_{c|x}} \mathcal{L}_{\text{Info}}(G, Q)$ . Here  $Q_{c|x}$  is an auxiliary conditional distribution, which is maximized over the InfoGAN regularizer defined as

$$\mathcal{L}_{\text{Info}}(G, Q) \triangleq \mathbb{E}_{c \sim P_c, z \sim P_z, x \sim G(z, c)} [\log Q_{c|x}] , \quad (3)$$

where  $P_c$  and  $P_z$  denote the distributions chosen as priors. When this lower bound is maximized over  $Q_{c|x}$ , it acts as a surrogate for mutual information: rearranging the terms gives

$$\mathcal{L}_{\text{Info}}(G, Q) = I(c; x) - H(c) - \mathbb{E}_{x \sim P_x} [d_{\text{KL}}(P_{c|x} \| Q_{c|x})] ,$$

and  $\max_{Q_{c|x}} \mathcal{L}_{\text{Info}}(G, Q) = I(c; x) - H(c)$  (see [8] for a derivation). However, this maximization is a functional optimization over an infinite dimensional function  $Q_{c|x}$ , which is intractable. To make this tractable, the optimization is done over a restricted family of Gaussian distributions in [8], which are factorized (or independent) Gaussian distributions (see  $\mathcal{Q}$  in Remark 1).  $Q_{c|x}$  can then be parametrized by the conditional means and variances, which is now finite dimensional functions, and one can use deep neural networks to approximate them. Note that the Shannon entropy  $H(c)$  is a constant that does not depend on  $G(\cdot, \cdot)$  or  $Q_{c|x}$ .

Next, if this maximum over  $Q_{c|x}$  has been achieved, then notice that in the generator update, the generator tries to minimize  $\min_G \mathcal{L}_{\text{Adv}}(G, D) - \lambda(I(c; x) - H(c))$ . This is problematic as the  $G$  update will increase  $I(c, x)$  unboundedly, tending to infinity (even if  $Q_{c|x}$  is restricted to factorized Gaussian class). The maximum value of  $I(c; x) = \infty$  is achieved, for example, if  $Q_{c_i|x}$  has variance zero for some  $i$ . This problem is not just theoretical. In Appendix B, we confirm experimentally that training InfoGAN with an unfactorized  $Q_{c|x}$  leads to training instability. To avoid such catastrophic failures, [8] forces  $Q_{c|x}$  to have an identity covariance matrix. This restricts the class of  $Q_{c|x}$  that we search over, and forces the  $\mathcal{L}_{\text{Info}}(G, Q)$  to be bounded, and the  $G$  and  $Q_{c|x}$  updates to be well-defined. In summary, for stability and efficiency of training, [8] restricted  $Q_{c|x}$  to be a *factorized Gaussian with identity covariance*. We show next that this choice creates an implicit bias.

**Remark 1.** *If optimized over a class of factorized Gaussian conditional distributions with unit variances, i.e.  $\mathcal{Q} = \{Q_{c|x} | Q_{c|x} = Q_{c_1|x} \times \dots \times Q_{c_k|x}\}$  and  $Q_{c_i|x} = (1/\sqrt{2\pi}) \exp\{-(1/2)(c_i - \mu_i(x))^2\}$  for some  $\mu_i(x) \in \mathbb{R}$  for all  $i \in [k]$  and  $x \in \mathcal{X}$ , the maximum of the InfoGAN loss in Eq. (3) has the following implicit bias:*

$$\max_{Q_{c|x} \in \mathcal{Q}} \mathcal{L}_{\text{Info}}(G, Q) = I(x; c) - H(c) - \underbrace{\mathbb{E} \left[ \log \frac{P_{c|x}}{N_{c_1|\nu_1(x)} \dots N_{c_k|\nu_k(x)}} \right]}_{\text{implicit bias}} , \quad (4)$$

where  $P_{c,x}$  is the joint distribution between the latent code  $c$  and the generated image  $x = G(c, z)$ , and  $N_{c_i|\nu_i(x)} = 1/\sqrt{2\pi} \exp\{-(1/2)(c_i - \nu_i(x))^2\}$  with  $\nu_i = \mathbb{E}_{P_{c_i|x}}[c_i]$  is the best one-dimensional Gaussian approximation of  $P_{c_i|x}$ .

We provide a proof in Appendix A. The above implicit bias keeps the loss bounded, so it is necessary. On the other hand, it might have undesired and unintended consequences in terms of learning a disentangled deep generative model. In this paper, we therefore introduce a new regularizer to explicitly encourage disentanglement during InfoGAN training.

**Improving InfoGAN performance via stable training.** Before introducing our proposed regularizer, note that several VAE-based architectures claim to outperform InfoGAN by significant margins [23, 17, 7]. This series of empirical results has created a misconception that InfoGAN is fundamentally limited in achieving disentanglement, which has been reinforced in following literature

[21, 4], which refer to those initial results. We show that the previously-reported inferior empirical performance of InfoGAN is due to poor architectural and hyperparameter choices in training. We take the same implementation reported to have bad performance (disentanglement score of 0.59 in Table 1). We then apply recently-proposed (but now popular) techniques for stabilizing GAN training and achieve a performance comparable to the best reported results of competing approaches (disentanglement score of 0.83 in Table 1). We provide more supporting experimental results in Section 4. Concretely, we start from the implementation in [23]. We then apply spectral normalization to the adversarial loss discriminator [31], with a choice of cross entropy loss, and use two time-scale update rule [16] with an appropriate choice of the learning rate. These choices are motivated by similar choices and successes of [6] in scaling GAN to extremely large datasets. Implementation details are in Appendix E.4, and we also submit the code for reproducibility. Hence, the starting point for our design is to achieve even better disentanglement than a properly-trained version of InfoGAN.

### 3 Contrastive regularizer

Based on the insights from Section 2, we introduce a *contrastive regularizer*. A new discriminator  $H$  encourages disentanglement and is added to the loss, for a positive scalar  $\alpha$ :

$$\min_{G,H} \max_D \mathcal{L}_{\text{Adv}}(G, D) - \lambda I(c; G(c, z)) - \alpha \mathcal{L}_c(G, H). \quad (5)$$

The key insight is that disentanglement is fundamentally measured by the *changes* made when traversing the latent space. Detecting changes inevitably requires the discriminator to make decisions based on multiple samples jointly. We propose generating multiple samples, whose latent codes are coupled. We design multiple hypotheses on how to couple those latent codes, and generate multiple examples from one of those hypotheses. The new discriminator  $H$  tries to detect which hypothesis the set of images are generated from. The key insight is to design those hypotheses in a way to encourage each latent code to make changes in the sample that are noticeable and distinct.

We progressively change the hypotheses during the course of the training, from easy to hard. The hypotheses class we propose is as follows. Both the generator and the discriminator try to make the following  $k$ -way hypothesis testing successful. First we draw a random index  $I$  over  $k$  indices, and sample the chosen latent code  $c_I \in \mathbb{R}$ . Two images are generated with the same value of  $c_I$ ; the remaining factors are chosen independently at random. Letting  $c_j^m$  denote the  $j$ th latent code for image  $m \in \{1, 2\}$ , the *contrastive gap* is defined as  $\min_{j \in [k] \setminus \{I\}} |c_j^1 - c_j^2|$ . The larger the contrastive gap, the more distinct the pair of samples. We gradually reduce the contrastive gap for progressive training (Section 4.1). This pair of coupled images  $x$  and  $x'$  are fed to the discriminator  $H$ , which tries to identify which code was shared. We use cross entropy loss:

$$\mathcal{L}_c(G, H) = \mathbb{E}_{I \sim \mathcal{U}([k]), (x, x') \sim Q^{(I)}} [\langle I, \log H(x, x') \rangle], \quad (6)$$

where  $Q^{(I)}$  denotes the joint distribution of the paired images,  $I$  denotes the one-hot encoding of the random index, and  $H$  is a  $k$ -dimensional vector-valued neural network normalized to be  $\langle \mathbf{1}, H(x, x') \rangle = 1$  for all  $x$  and  $x'$ . This encourages each latent code to make distinct and noticeable changes, hence promoting disentanglement. This architecture is illustrated in Figure 1. An alternative interpretation of the proposed loss as a divergence is provided in Appendix C.

## 4 Experiments

We run experiments on a combination of synthetic datasets with pre-defined latent factors and real-world datasets.<sup>5</sup> In our experiments, we evaluate two properties: disentanglement and image quality. For image quality, we use the common *inception score* metric. For disentanglement, we use the popular metric proposed by Kim and Mnih in [23]. This metric is a number between zero and one, with one being a perfect disentanglement. We additionally compute the (less common) disentanglement metric of [12]. We give a full description of all metrics in Appendix D.



Figure 3: Example images from the dSprites dataset.

<sup>5</sup>The code for all experiments is available at <https://github.com/fjxmlzn/InfoGAN-CR>

	Model	Disentanglement (Kim & Mnih)	Disentanglement (Eastwood & Williams)
VAE	VAE ( $\beta = 1.0$ )	$0.63 \pm 0.06$	$0.30 \pm 0.10$
	$\beta$ -TCVAE ( $\beta = 4.0$ )	$0.62 \pm 0.07$	$0.29 \pm 0.10$
	HFVAE ( $\beta = 4.0, \gamma = 3.0$ )	$0.63 \pm 0.08$	$0.39 \pm 0.16$
	$\beta$ -VAE ( $\beta = 4.0$ )	$0.63 \pm 0.10$	$0.41 \pm 0.11$
	CHyVAE	0.77	
	FactorVAE*	0.82	<b><math>0.74 \pm 0.01</math></b>
GAN	InfoGAN*	$0.59 \pm 0.70$	$0.41 \pm 0.05$
	IB-GAN	$0.80 \pm 0.07$	$0.67 \pm 0.07$
	InfoGAN (modified)*	$0.83 \pm 0.03$	$0.56 \pm 0.03$
	InfoGAN-CR* (ours)	<b><math>0.90 \pm 0.01</math></b>	<b><math>0.74 \pm 0.01</math></b>

Table 1: Comparisons of the disentanglement metric proposed in [23] on the dSprites dataset. A perfect disentanglement corresponds to 1.0 score. The proposed InfoGAN-CR achieves the highest score, compared to the best reported result for each baseline from [23, 21, 13, 4, 28]. The value for CHyVAE is obtained from [4]; Kim & Mnih value for FactorVAE is obtained from [23]; Eastwood & Williams value for FactorVAE is from ourselves; and the remaining disentanglement scores for baseline approaches are obtained from [21]. Asterisks denote experiments that we ran or confirmed ourselves. See Appendix E.4 for InfoGAN (modified).

#### 4.1 dSprites Dataset

We begin with the synthetic dSprites dataset [30], commonly used to numerically compare disentangling methods. The dataset consists of 737,280 binary  $64 \times 64$  images of 2D shapes generated from five ground truth independent latent factors: color, shape, scale, rotation, x and y position. All combinations of latent factors are present in the dataset; some examples are illustrated in Figure 3. Figure 1 illustrates the latent traversal for InfoGAN-CR. To generate this figure, we fix all latent factors except one  $c_i$ , and vary  $c_i$  from -1 to 1 in evenly-spaced intervals. We observe that each of the five empirically-learned factors captures one true underlying factor, and the traversals span the full range of possibilities for each hidden factor.

We compute and/or reproduce disentanglement metrics for a number of protocols in Table 1. In this table, all algorithms with an asterisk were either run or independently confirmed by us. For the metric of [23], Table 1 shows that the baseline disentanglement of InfoGAN can be substantially boosted through better training, from 0.59 to 0.83. Contrastive regularization provides an additional gain, bringing InfoGAN-CR’s disentanglement up to 0.90, higher than any baseline from the VAE or GAN literature. For the metric of [12], we find similar trends, except FactorVAE is tied with InfoGAN-CR for the best score. We were made aware of independent work that proposes a similar idea to contrastive regularization in [26]. Their algorithm is a special case of contrastive regularization, which empirically achieves lower disentanglement scores ( $0.39 \pm 0.02$  standard error over 10 runs) than even vanilla InfoGAN. For this reason, we do not consider it as a baseline moving forward. Note that this discrepancy is not a matter of parameter tuning, but of the loss function; indeed, in our own preliminary trials, we found that training a CR-regularizer without the InfoGAN loss achieved similarly poor performance, as described in Appendix E.3. Concretely, [26] fixes  $\lambda = 0$  in our loss (5), and also uses a special coupling that matches all but one latent code in  $c$  for the matched pairs. In combination, these choices result in a significant degradation of performance.

We implemented both FactorVAE and InfoGAN using the architectures described in [23]. For completeness, we describe both architectures in detail in Appendix E.4. Although InfoGAN exhibits a reported disentanglement score of  $0.59 \pm 0.70$  in [23], we find that InfoGAN can exhibit substantially higher disentanglement scores ( $0.83 \pm 0.03$ ) through some basic changes to the architecture and loss function. In particular, in accordance with [31], we changed the loss function from Wasserstein GAN to the traditional JSD loss. We also changed the generator’s Adam learning rate to 0.001 and the InfoGAN and CR discriminators learning rates to 0.002; we used 5 continuous input codes, whereas [23] reported using four continuous codes and one discrete one. We also used batch normalization in the generator, and spectral normalization in the discriminator. Finally, we used InfoGAN regularizer  $\lambda = 0.05$ , and for InfoGAN-CR, we used contrastive regularizer  $\alpha = 2.0$ . The effects of these changes are shown in the line ‘InfoGAN (modified)’ in Table 1. For FactorVAE,

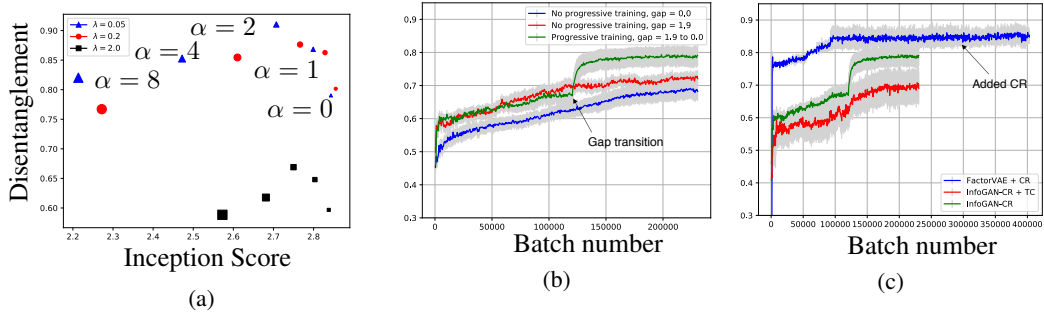


Figure 4: (left) Achievable (inception score, disentanglement) pairs for InfoGAN-CR, varying the contrastive regularizer  $\alpha$  and the InfoGAN regularizer  $\lambda$ . The size of each point denotes  $\alpha \in \{0, 1, 2, 4, 8\}$ , in order of increasing size; we have explicitly labelled this for  $\lambda = 0.05$  (blue triangles). The inception score of groundtruth data is 2.94. (center) Reducing the contrastive gap from 1.9 to 0 during training gives better disentanglement scores than either fixed gap. (right) Adding TC regularization to InfoGAN-CR does not improve disentanglement; neither does adding CR to FactorVAE.

we used the architecture of [23], which uses  $k = 10$  latent codes in their architecture. To compute disentanglement, we use the metric of [23].

**Parameters.** We start by showing the effect of varying InfoGAN-CR’s parameters: the InfoGAN regularizer  $\lambda$  and the contrastive regularizer  $\alpha$ . In particular, we are interested in understanding how these parameters trade off disentanglement with image quality. To this end, we vary both parameters and compute both the disentanglement metric of [23] and inception score [37], explained in detail in Appendix D. Since inception scores can only be computed for labelled, categorical data, we compute it over the ‘shape’ latent factor, which has three options: heart, square, or oval. Figure 4a shows the resulting trends, both for InfoGAN-CR and for modified InfoGAN (which is a special case with  $\alpha = 0$ ). For InfoGAN-CR, we set  $\lambda \in \{0.05, 0.2, 2.0\}$  and take  $\alpha \in \{0, 1, 2, 4, 8\}$ . The size of each point in Figure 4a corresponds to the value of  $\alpha$ , which we explicitly label for  $\lambda = 0.05$  (blue triangles). Each data point is averaged over 11 runs. As we increase the contrastive regularizer, inception score decreases, whereas disentanglement improves up to a point, and then decreases. Notably, using contrastive regularizer  $\alpha = 1$  or  $\alpha = 2$  seems to incur small reductions in inception score for a significant boost in disentanglement. To better understand these results, we generated similar plots using more nuanced image quality metrics, included in Appendices D and E.1.

**Progressive Training.** One key aspect of contrastive regularization is its progressive reduction of the contrastive gap during training. In this section, we show the importance of progressive training by comparing it to regularization for a fixed gap. Figure 4b shows the disentangling metric of [23] as a function of batch number. For the ‘progressive training’ curve, we use a contrastive gap of 1.9 for 120,000 batches, and then introduce a (more aggressive) gap of 0. For the ‘no progressive training’ curves, we use gap size of 0 or 1.9 for all 230,400 batches. All curves use an InfoGAN regularizer  $\lambda = 0.7$  and a CR weight  $\alpha = 1.0$ . Notice that the results in Table 1 were computed for a different value of  $\lambda$ , which explains why Figure 4b achieves lower disentanglement scores. The ‘no progressive training, gap=0.0’ curve is averaged over 21 runs whereas the rest two curves are averaged over 10 runs.

We observe that progressive training helps the disentanglement metric grow faster than either setting without progressive training. We also tried a smooth progressive training schedule (e.g. smoothly decreasing the contrastive gap), but found this to hurt the disentanglement performance. In both cases, we found that re-randomizing the CR-discriminator’s parameters every time the contrastive gap was changed helped to stabilize training.

**Objective Function.** We claim that contrastive regularization is tailored to work well with GAN architectures. Similarly, we claim that total correlation regularization of FactorVAE is specifically tailored for VAE. To test this hypothesis, we have applied contrastive regularization (CR) to FactorVAE

Scheme	Disentanglement
FactorVAE ( $\beta = 1$ )	$0.65 \pm 0.04$
FactorVAE ( $\beta = 10$ )	$0.62 \pm 0.03$
FactorVAE ( $\beta = 20$ )	$0.67 \pm 0.04$
FactorVAE ( $\beta = 40$ )	$0.79 \pm 0.03$
InfoGAN (modified, $\lambda = .2$ )	$0.76 \pm 0.06$
InfoGAN-CR ( $\lambda = .2, \alpha = 3$ )	<b><math>0.86 \pm 0.03</math></b>

Table 2: Disentanglement metric [23] for teapot dataset.

and total correlation (TC) regularization to InfoGAN-CR. Figure 4c shows the disentanglement metric of each as a function of batch numbers. For FactorVAE, we introduce CR regularization of  $\alpha = 20$  at batch 300,000. Note that the metric does not change perceptibly after adding CR. For InfoGAN-CR, we ran one set of trials with TC regularization from the beginning (red curve) and one set of trials without TC regularization (green curve). We use InfoGAN regularizer  $\lambda = 0.7$  and TC coefficient  $\beta = 1$  for the former. Notice that InfoGAN-CR has a lower disentanglement score than FactorVAE in this plot because we did not use the optimal  $\lambda$  for this dataset; this sensitivity is a weakness of InfoGAN-CR (as well as InfoGAN). In Figure 4c, we observe that TC regularization actually reduces disentanglement compared to InfoGAN-CR without TC. The jumps in disentanglement for the InfoGAN-CR curves are due to progressive training; we change the contrastive gap from 1.9 to 0.0 at batch 120,000. The red line (InfoGAN-CR + TC) is averaged over 4 runs, the blue line (FactorVAE + CR) over 2 runs, and the green line (InfoGAN-CR) over ten. These results support (but do not prove) our hypothesis that CR is better-suited to GAN architectures, whereas TC is better-suited to VAE architectures. To further confirm this intuition, we show that disentanglement appears negatively correlated with a measure of total correlation in Appendix E.2.

## 4.2 Teapots Dataset

We ran InfoGAN-CR on the teapots dataset from [12], with images of teapots in various orientations and colors generated by the renderer in [32]. Images have five latent factors: color (red, blue, and green), rotation (vertical), and rotation (lateral). Colors are randomly drawn from  $[0, 1]$ . Rotation (vertical) is randomly drawn from  $[0, \pi/2]$ . Rotation (lateral) is drawn from  $[0, 2\pi]$ . We generated a dataset of 200,000 such images with each combination of latent factors represented. Table 2 shows the disentanglement scores of FactorVAE and InfoGAN compared to InfoGAN-CR. Again, we observe that InfoGAN-CR achieves a higher disentanglement score than the other baselines, and contrastive regularization increases the metric compared to modified InfoGAN. Since the teapots dataset does not have classes, we do not compute inception score for this dataset; however, the images generated by InfoGAN-CR appear sharper than those generated by FactorVAE. Details on this point, our implementation, and additional plots appear in Appendix F.

## 4.3 CelebA Dataset

Finally, we tested InfoGAN-CR on the CelebA dataset to observe its performance on real-world data. CelebA is a dataset of 202599 facial images from celebrities. Since these images do not have known latent factors or labelled categories, we cannot compute the disentanglement metric or inception score. We therefore evaluate this dataset qualitatively by producing latent traversals, as seen in Figure 5. Details of this experiment are included in Appendix H.

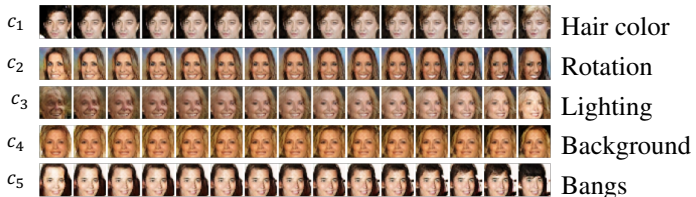


Figure 5: Latent traversal for CelebA dataset, using InfoGAN-CR.



## 5 Conclusion

In this work, we propose contrastive regularization (CR) for improving the disentanglement performance of GAN-based generative models. Our main finding is that GAN-based disentanglement methods can substantially outperform state-of-the-art, VAE-based methods. In addition, we experimentally find that CR substantially increases the disentanglement capabilities of InfoGAN, but does not appear to affect the state-of-the-art VAEs. Similarly, we experimentally show that the total correlation regularization, a popular technique for disentangling VAEs, do not improve disentanglement in GAN training. This suggests that disentangling VAEs and GANs require fundamentally different techniques. The proposed CR regularization could be used in any application to enhance disentanglement of GANs, for example in hierarchical image representation or reinforcement learning. Understanding this phenomenon analytically is an interesting direction for future work, and may give rise to a more general understanding of how to design regularizers for GANs as opposed to VAEs. Another key question is to understand disentanglement in challenging datasets, compared to those studied in the literature as a benchmark. We study two such datasets. The first one studies three dimensional rotations on the teapots dataset in Appendix F.1. Existing training datasets includes only a subset of the full rotations, making disentanglement substantially easy. When training data is drawn from complete set of rotations in 3-D space, several challenges arise. The usual rotations along the three standard basis vectors do not commute, hence do not disentangle. We can find a commutative coordinate system, but it is not uniquely defined. Our preliminary experiments suggest that current state-of-the-art methods fail to learn a disentangled representation. The second one studies two dimensional polar coordinate system in Appendix G. State-of-the-art methods fail to learn the disentangled representation of the polar coordinates.

## Acknowledgements

The authors would like to thank Qian Ge for valuable discussions about InfoGAN architecture.

This work is supported by NSF awards 1927712, 1705007, and 1815535 and Google Faculty Research Award. This work used the Extreme Science and Engineering Discovery Environment (XSEDE), which is supported by National Science Foundation grant number OCI-1053575. Specifically, it used the Bridges system, which is supported by NSF award number ACI-1445606, at the Pittsburgh Supercomputing Center (PSC). This work is partially supported by the generous research credits on AWS cloud computing resources from Amazon and funding from Siemens.

## References

- [1] Samuel K Ainsworth, Nicholas J Foti, and Emily B Fox. Disentangled vae representations for multi-aspect and missing data. *arXiv preprint arXiv:1806.09060*, 2018.
- [2] Samuel K. Ainsworth, Nicholas J. Foti, Adrian K. C. Lee, and Emily B. Fox. oi-VAE: Output interpretable VAEs for nonlinear group factor analysis. In *Proceedings of the 35th International Conference on Machine Learning*, volume 80, pages 119–128, 2018.
- [3] Mark A Aizerman. Theoretical foundations of the potential function method in pattern recognition learning. *Automation and remote control*, 25:821–837, 1964.
- [4] Abdul Fatir Ansari and Harold Soh. Hyperprior induced unsupervised disentanglement of latent representations. *arXiv preprint arXiv:1809.04497*, 2018.
- [5] Yoshua Bengio, Aaron Courville, and Pascal Vincent. Representation learning: A review and new perspectives. *IEEE transactions on pattern analysis and machine intelligence*, 35(8): 1798–1828, 2013.
- [6] Andrew Brock, Jeff Donahue, and Karen Simonyan. Large scale gan training for high fidelity natural image synthesis. *arXiv preprint arXiv:1809.11096*, 2018.
- [7] Tian Qi Chen, Xuechen Li, Roger Grosse, and David Duvenaud. Isolating sources of disentanglement in variational autoencoders. *arXiv preprint arXiv:1802.04942*, 2018.

- [8] Xi Chen, Yan Duan, Rein Houthoofd, John Schulman, Ilya Sutskever, and Pieter Abbeel. Infogan: Interpretable representation learning by information maximizing generative adversarial nets. In *Advances in Neural Information Processing Systems*, pages 2172–2180, 2016.
- [9] Taco S Cohen and Max Welling. Transformation properties of learned visual representations. *arXiv preprint arXiv:1412.7659*, 2014.
- [10] Guillaume Desjardins, Aaron Courville, and Yoshua Bengio. Disentangling factors of variation via generative entangling. *arXiv preprint arXiv:1210.5474*, 2012.
- [11] Emilien Dupont. Joint-vae: Learning disentangled joint continuous and discrete representations. *arXiv preprint arXiv:1804.00104*, 2018.
- [12] Cian Eastwood and Christopher KI Williams. A framework for the quantitative evaluation of disentangled representations. 2018.
- [13] Babak Esmaeili, Hao Wu, Sarthak Jain, Alican Bozkurt, N Siddharth, Brooks Paige, Dana H Brooks, Jennifer Dy, and Jan-Willem van de Meent. Structured disentangled representations. *stat*, 1050:12, 2018.
- [14] Shuyang Gao, Rob Brekelmans, Greg Ver Steeg, and Aram Galstyan. Auto-encoding total correlation explanation. *arXiv preprint arXiv:1802.05822*, 2018.
- [15] Ian Goodfellow, Jean Pouget-Abadie, Mehdi Mirza, Bing Xu, David Warde-Farley, Sherjil Ozair, Aaron Courville, and Yoshua Bengio. Generative adversarial nets. In *Advances in neural information processing systems*, pages 2672–2680, 2014.
- [16] Martin Heusel, Hubert Ramsauer, Thomas Unterthiner, Bernhard Nessler, and Sepp Hochreiter. Gans trained by a two time-scale update rule converge to a local nash equilibrium. In *Advances in Neural Information Processing Systems 30*, pages 6629–6640. 2017.
- [17] Irina Higgins, Loic Matthey, Arka Pal, Christopher Burgess, Xavier Glorot, Matthew Botvinick, Shakir Mohamed, and Alexander Lerchner. beta-vae: Learning basic visual concepts with a constrained variational framework. 2016.
- [18] Irina Higgins, Arka Pal, Andrei A Rusu, Loic Matthey, Christopher P Burgess, Alexander Pritzel, Matthew Botvinick, Charles Blundell, and Alexander Lerchner. Darla: Improving zero-shot transfer in reinforcement learning. *arXiv preprint arXiv:1707.08475*, 2017.
- [19] Irina Higgins, David Amos, David Pfau, Sebastien Racaniere, Loic Matthey, Danilo Rezende, and Alexander Lerchner. Towards a definition of disentangled representations. *arXiv preprint arXiv:1812.02230*, 2018.
- [20] Irina Higgins, Nicolas Sonnerat, Loic Matthey, Arka Pal, Christopher P Burgess, Matko Bošnjak, Murray Shanahan, Matthew Botvinick, Demis Hassabis, and Alexander Lerchner. Scan: Learning hierarchical compositional visual concepts. 2018.
- [21] Insu Jeon, Wonkwang Lee, and Gunhee Kim. Ib-gan: Disentangled representation learning with information bottleneck gan. 2018.
- [22] Theofanis Karaletsos, Serge Belongie, and Gunnar Rätsch. Bayesian representation learning with oracle constraints. *arXiv preprint arXiv:1506.05011*, 2015.
- [23] Hyunjik Kim and Andriy Mnih. Disentangling by factorising. In *International Conference on Machine Learning*, 2018.
- [24] Diederik P Kingma and Max Welling. Auto-encoding variational bayes. *arXiv preprint arXiv:1312.6114*, 2013.
- [25] Tejas D Kulkarni, William F Whitney, Pushmeet Kohli, and Josh Tenenbaum. Deep convolutional inverse graphics network. In *Advances in neural information processing systems*, pages 2539–2547, 2015.
- [26] Zejian Li, Yongchuan Tang, and Yongxing He. Unsupervised disentangled representation learning with analogical relations. *arXiv preprint arXiv:1804.09502*, 2018.

- [27] Zinan Lin, Ashish Khetan, Giulia Fanti, and Sewoong Oh. Pacgan: The power of two samples in generative adversarial networks. *arXiv preprint arXiv:1712.04086*, 2017.
- [28] Francesco Locatello, Stefan Bauer, Mario Lucic, Sylvain Gelly, Bernhard Schölkopf, and Olivier Bachem. Challenging common assumptions in the unsupervised learning of disentangled representations. *arXiv preprint arXiv:1811.12359*, 2018.
- [29] Romain Lopez, Jeffrey Regier, Michael I Jordan, and Nir Yosef. Information constraints on auto-encoding variational bayes. In S. Bengio, H. Wallach, H. Larochelle, K. Grauman, N. Cesa-Bianchi, and R. Garnett, editors, *Advances in Neural Information Processing Systems 31*, pages 6117–6128. 2018.
- [30] Loic Matthey, Irina Higgins, Demis Hassabis, and Alexander Lerchner. dsprites: Disentanglement testing sprites dataset. 2017. <https://github.com/deepmind/dsprites-dataset/>.
- [31] Takeru Miyato, Toshiki Kataoka, Masanori Koyama, and Yuichi Yoshida. Spectral normalization for generative adversarial networks. In *International Conference on Learning Representations (ICLR)*, 2018.
- [32] Pol Moreno, Christopher KI Williams, Charlie Nash, and Pushmeet Kohli. Overcoming occlusion with inverse graphics. In *European Conference on Computer Vision*, pages 170–185. Springer, 2016.
- [33] Siddharth Narayanaswamy, T. Brooks Paige, Jan-Willem van de Meent, Alban Desmaison, Noah Goodman, Pushmeet Kohli, Frank Wood, and Philip Torr. Learning disentangled representations with semi-supervised deep generative models. In *Advances in Neural Information Processing Systems 30*, pages 5925–5935. 2017.
- [34] Niklas Pfister, Peter Bühlmann, Bernhard Schölkopf, and Jonas Peters. Kernel-based tests for joint independence. *Journal of the Royal Statistical Society: Series B (Statistical Methodology)*, 80(1):5–31, 2018.
- [35] Edouard Pineau and Marc Lelarge. Infocatvae: Representation learning with categorical variational autoencoders. *arXiv preprint arXiv:1806.08240*, 2018.
- [36] Karl Ridgeway. A survey of inductive biases for factorial representation-learning. *arXiv preprint arXiv:1612.05299*, 2016.
- [37] Tim Salimans, Ian Goodfellow, Wojciech Zaremba, Vicki Cheung, Alec Radford, and Xi Chen. Improved techniques for training gans. In *Advances in Neural Information Processing Systems*, pages 2234–2242, 2016.
- [38] Jürgen Schmidhuber. Learning factorial codes by predictability minimization. *Neural Computation*, 4(6):863–879, 1992.
- [39] Akash Srivastava, Lazar Valkov, Chris Russell, Michael Gutmann, and Charles Sutton. Vee-gan: Reducing mode collapse in gans using implicit variational learning. *arXiv preprint arXiv:1705.07761*, 2017.
- [40] Christian Szegedy, Vincent Vanhoucke, Sergey Ioffe, Jon Shlens, and Zbigniew Wojna. Rethinking the inception architecture for computer vision. In *Proceedings of the IEEE conference on computer vision and pattern recognition*, pages 2818–2826, 2016.
- [41] Yichuan Tang, Ruslan Salakhutdinov, and Geoffrey Hinton. Tensor analyzers. In *International Conference on Machine Learning*, pages 163–171, 2013.

## Appendix

### A Proof of Remark 1

Notice that  $\mathcal{L}_{\text{Info}}(G, Q) \leq I(c, G(z, c))$ . To understand why this works, let us decompose this lower bound further:

$$\begin{aligned}
\mathcal{L}_{\text{Info}}(G, Q) &= \mathbb{E}_{c \sim P_c, z \sim P_z, x \sim G(z, c)} [\log Q_{c|x}] \\
&= \mathbb{E}_{(x, c) \sim P(x, c)} [\log Q_{c|x}] \\
&= I(x; c) - H(c) + \mathbb{E}_{(x, c) \sim P(x, c)} \left[ \log \frac{Q_{c|x} P_x}{P_x P_{c|x}} \right] \\
&= I(x; c) - H(c) + \mathbb{E}_{(x, c) \sim P(x, c)} \left[ \log \frac{Q_{c|x}}{P_{c|x}} \right] \\
&= I(c; x) - H(c) - \mathbb{E}_{x \sim P_x} [d_{\text{KL}}(P_{c|x} \| Q_{c|x})]
\end{aligned}$$

We can further simplify and maximize the last term, which is the only one dependent on  $Q$  as,

$$\begin{aligned}
&\min_{Q \in \mathcal{Q}} \mathbb{E}_{x \sim P_x} [d_{\text{KL}}(P_{c|x} \| Q_{c|x})] \\
&= \min_{Q \in \mathcal{Q}} \mathbb{E}_{c, x \sim P_{c, x}} \left[ \log \left( \frac{P_{c|x}}{Q_{c|x}} \right) \right] \\
&= \min_{Q \in \mathcal{Q}} \mathbb{E}_{c, x \sim P_{c, x}} \left[ \log \left( \frac{P_{c|x}}{N_{c_1|\nu_1(x)} \cdots N_{c_k|\nu_k(x)}} \right) + \log \left( \frac{N_{c_1|\nu_1(x)} \cdots N_{c_k|\nu_k(x)}}{Q_{c|x}} \right) \right] \\
&= \mathbb{E}_{c, x \sim P_{c, x}} \left[ \log \left( \frac{P_{c|x}}{N_{c_1|\nu_1(x)} \cdots N_{c_k|\nu_k(x)}} \right) \right] + \min_{Q \in \mathcal{Q}} \mathbb{E}_{c, x \sim P_{c, x}} \left[ \log \left( \frac{N_{c_1|\nu_1(x)} \cdots N_{c_k|\nu_k(x)}}{Q_{c|x}} \right) \right] \\
&= \mathbb{E}_{c, x \sim P_{c, x}} \left[ \log \left( \frac{P_{c|x}}{N_{c_1|\nu_1(x)} \cdots N_{c_k|\nu_k(x)}} \right) \right],
\end{aligned}$$

where the last equality follows from the fact that any  $Q \in \mathcal{Q}$  can be parametrized by  $(\mu_1(x), \dots, \mu_k(x))$  as  $Q_{c|x} = Q_{c_1|x} \cdots Q_{c_k|x}$  with  $Q_{c_i|x} = (1/\sqrt{2\pi}) \exp\{-(1/2)(c_i - \mu_i(x))^2\}$ , in which case

$$\begin{aligned}
\min_{Q \in \mathcal{Q}} \mathbb{E}_{c, x \sim P_{c, x}} \left[ \log \left( \frac{N_{c_1|\nu_1(x)} \cdots N_{c_k|\nu_k(x)}}{Q_{c|x}} \right) \right] &= \min_{\{\mu_i(x)\}_{i=1}^k} \mathbb{E}_{x \sim P_x} \left[ \sum_{i \in [k]} (\mu_i(x) - \nu_i(x))^2 \right] \\
&\geq 0,
\end{aligned}$$

and the minimum of zero can be achieved by  $\mu_i(x) = \nu_i(x)$ , where  $\nu_i(x) = \mathbb{E}_{P_{c|x}}[c_i]$ .

### B InfoGAN with non-factorizing decoder

In this section we verify that the InfoGAN trained with non-factorizing multi-variate Gaussian distribution  $Q(c|x)$  is unstable. Specifically, we train an InfoGAN with a decoder distribution of  $Q(c|x) = \mathcal{N}(\mu(x), \Sigma(x))$ , where  $\mathcal{N}$  is the multivariate Gaussian distribution with mean  $\mu(x) \in \mathbb{R}^k$ , and full covariance matrix  $\Sigma(x) \in \mathbb{R}^{k \times k}$ . These parameters of the distribution are modelled as neural network functions of  $x$ , where we explicitly enforce the positive semi-definiteness of  $\Sigma(x)$ . This is less restrictive than the factorizing decoder distribution,  $Q(c|x) = \prod_{i \in [k]} Q(c_i|x) = \prod_{i \in [k]} \mathcal{N}(\mu_i(x), 1)$  with its fixed diagonal covariance matrix  $\mathbb{I}$ , in the standard InfoGAN (see Remark 1).

Figure 6 shows the degradation in disentanglement due to the non-factorizing decoder. Similar to the experiment in Figure 2, we first train the standard InfoGAN ( $\lambda = 0.2$ ) with factorizing decoder distribution  $Q(c|x) = \prod_{i \in [k]} \mathcal{N}(\mu_i(x), 1)$  on dSprites dataset for 25 epochs (288,000 batches) and from this point onwards we train two different versions of this model for 3 more epochs: one where we continue training the standard InfoGAN (blue solid curve) and another version where we replace the non-factorizing decoder distribution with the factorizing decoder distribution

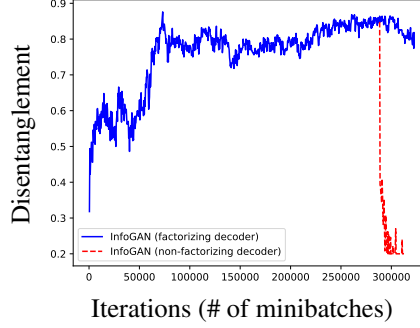


Figure 6: After 288,000 iterations, we continue training an InfoGAN with/without the non-factorizing decoder distribution  $Q(c|x)$  (Section B). Non-factorizing decoder is high unstable and its training terminates early after reaching a low values of 0.2.

$Q(c|x) = \mathcal{N}(\mu(x), \Sigma(x))$  (red dashed curve). We plot the disentanglement metric, as defined in Section 4.

We see that the non-factorizing decoder is highly unstable and its performance drops (from that of factorizing decoder) to 0.2 (minimum possible value for 5 latent codes) and its training terminates early because the learnt covariance matrix  $\Sigma(x)$  becomes rank deficient.

## C Alternative interpretation of the CR loss

An alternative interpretation of the proposed loss is as a divergence over the distributions of the test examples. The discriminator, with an enough representation power, provides an approximation of the generalized Jensen-Shannon divergence (as shown below). The generator, in the subsequent generator update, forces the  $Q^{(i)}$ 's to be as different as possible, as measured by the provided JS divergence. This, in turn, forces the changes in the latent codes to make changes in the images that are noticeable and easy to distinguish from (the changes of) other latent codes.

**Remark 2.** When maximized over the class of all functions, the maximum in Eq. (6) is achieved by  $H(x, x') = (1/Z_{x, x'}) [Q^{(1)}(x, x'), \dots, Q^{(k)}(x, x')]$  with a normalizing constant  $Z_{x, x'} = \sum_{i \in [k]} Q^{(i)}(x, x')$  and the maximum value is the generalized Jensen-Shannon divergence up to a shift by a constant that only depends on  $k$ :

$$d_{\text{JS}}(Q^{(1)}, \dots, Q^{(k)}) \triangleq \frac{1}{k} \sum_{i \in [k]} d_{\text{KL}} \left( Q^{(i)} \parallel \frac{\sum_{j \in [k]} Q^{(j)}}{k} \right).$$

*Proof.* The solution to the following optimization problem is  $H(x, x') = (1/Z_{x, x'}) [Q^{(1)}(x, x'), \dots, Q^{(k)}(x, x')]$  with a normalizing constant  $Z_{x, x'} = \sum_{i \in [k]} Q^{(i)}(x, x')$ .

$$\begin{aligned} \arg \max_H & \quad \mathbb{E}_{I \sim \text{Unif}([k]), (x, x') \sim Q^{(I)}} [\langle I, \log H(x, x') \rangle], \\ \text{subject to} & \quad \langle \mathbf{1}, H(x, x') \rangle = 1, \text{ for all } (x, x'). \end{aligned}$$

This follows from the fact that the gradient of the Lagrangian is  $Q^{(i)}(x, x')/H_i(x, x') - \mu_{x, x'}$  where  $\mu_{x, x'}$  is the Lagrangian multiplier, and setting it to zero gives the desired maximizer. Plugging this

back into the objective function, we get that

$$\begin{aligned}
& \max_{\|H(x,x')\|_1=1} \mathbb{E}[\langle I, \log H(x, x') \rangle] \\
&= \frac{1}{k} \sum_{i \in [k]} \mathbb{E}_{(x,x') \sim Q^{(i)}} \left[ \log \frac{Q^{(i)}(x, x')/k}{\sum_{j \in [k]} Q^{(j)}(x, x')/k} \right] \\
&= \frac{1}{k} \sum_{i \in [k]} d_{\text{KL}} \left( Q^{(i)} \parallel \frac{\sum_{j \in [k]} Q^{(j)}}{k} \right) - \log k \\
&= d_{\text{JS}}(Q^{(1)}, \dots, Q^{(k)}) - \log k.
\end{aligned}$$

□

## D Evaluating performance

We use the following metrics to evaluate various aspects of the trained latent representation: disentanglement, independence, and generated image quality.

**Disentanglement** We use the popular disentanglement metric proposed in [23]. This metric is defined for datasets with known ground truth factors and is computed as follows. First, generate data points where the  $i$ th factor is fixed, but the other factors are varying uniformly at random, for a randomly-selected  $i$ . Pass each sample through the encoder, and normalize each resulting dimension by its empirical variance. Take the resulting dimension  $j$  with the smallest variance. In a setting with perfect disentanglement, the variance in the  $j$ th dimension would be 0. Each sample’s encoding generates a ‘vote’  $j$ ; we take the majority vote as the final output of the classifier; if the classifier is correct, it should map to  $i$ . The disentanglement metric is the error rate of this classifier, taken over many independent trials of this procedure. In our experiment, for each fixed factor index  $i$ , we generate 100 groups of images, where each group has 100 images with the same value at the  $i$ th index.

One challenge is computing the disentanglement metric for FactorVAE when trained with more latent codes  $k$  than there are latent factors (let  $\hat{k}$  denote the true number of factors). For instance, [23] uses  $c \in \mathbb{R}^{10}$  for datasets with only five latent codes. To account for this, [23] first removes all latent codes that have collapsed to the prior (i.e.,  $Q_{c_j|x} = P_{c_j}$ ); they then use the majority vote on the remaining factors. However, this approach can artificially change the metric if the number of factors for which the posterior does not equal the prior does not equal  $\hat{k}$ . Hence to measure the metric on FactorVAE (or more generally, cases where  $k > \hat{k}$ ), we first compute the  $k \times \hat{k}$  metric matrix, find the maximum value of each row. We then take the top  $\hat{k}$  among the  $k$  maximum row values, and sum them up.

We additionally compute the (less common) disentanglement metric of [12]. This metric first requires an estimate of the disentangled code  $\tilde{c}$  from the generated samples, for which we use our encoder. Next, we train a regressor  $f$  to predict  $c$  from  $\tilde{c}$ , so  $\hat{c} = f(\tilde{c})$ . These regressors must also provide a matrix of relative importance  $R$ , such that  $R_{ij}$  denotes the relative importance of  $\tilde{c}_i$  in predicting  $\hat{c}_j$ . Because of this requirement, Eastwood and Williams propose using regressors that provide importance scores, such as LASSO and random forests. These restrictions limit the generality of the metric; nonetheless, we include it for completeness. Given the regression  $f$ , disentanglement is computed for the  $i$ th latent code as  $D_i = (1 - H(W_{i,\cdot}))$  where  $H(\cdot)$  is the entropy of  $W_{i,\cdot}$  and  $W_{ij} = R_{ij} / \sum_{\bar{k}=0}^k R_{i\bar{k}}$ . The final disentanglement score is  $D = \frac{1}{k} \sum_i D_i$ .

Eastwood and Williams disentanglement metric is computed using the random forest regressor [12]<sup>6</sup>, as implemented in the `scikit-learn` library<sup>7</sup> with default values for all parameters, except for the `max_depth` parameter for which we use the values: 4, 2, 4, 2, and 2, for the latent factors: shape, scale, rotation,  $x$ -position, and  $y$ -position respectively, as used by the IB-GAN paper [21] (as per a private communication with its authors).

<sup>6</sup><https://github.com/cianeastwood/qedr/blob/master/quantify.ipynb>

<sup>7</sup><https://scikit-learn.org/stable/modules/generated/sklearn.ensemble.RandomForestRegressor.html>

**$d$ -Variable Hilbert-Schmidt Independence Score (dHSIC)** The dHSIC score is an empirical, kernel-based measure of the total correlation of a multivariate random variable from samples [34]. It is used in [29] to enforce independence among latent factors. We use this metric to understand whether and how disentanglement is correlated with total correlation. Suppose we have  $c \in \mathbb{R}^k$ . We want to compute the distance of the distribution  $P_c$  from the product distribution of the marginals  $\prod_i P_{c_i}$ . The dHSIC score over  $n$  samples is computed as follows. Consider a Gaussian kernel [3] with a median heuristic for bandwidth:

$$K_h(x_i, x_j) = e^{-\frac{\|x_i - x_j\|}{h^2}},$$

where  $h = \text{Median}(\{\|x_i - x_j\|\}_{i \neq j})$ . When there are  $k$  latent codes  $c_1, \dots, c_k$  and  $n$  samples, we have

$$\begin{aligned} \text{dHSIC}_n &= \frac{1}{n^2} \sum_{i,j \in [n]} \left( \prod_{\ell=1}^k K_{h_\ell}(c_{\ell i}, c_{\ell j}) \right) \\ &+ \frac{1}{n^{2k}} \prod_{\ell=1}^k \sum_{i,j \in [n]} K_{h_\ell}(c_{\ell i}, c_{\ell j}) - \frac{2}{n^{k+1}} \sum_{i \in [n]} \prod_{\ell=1}^k \sum_j K_{h_\ell}(c_{\ell i}, c_{\ell j}). \end{aligned}$$

**Image Quality** *Inception score* was first proposed in [37] for labelled data, and is computed as  $\exp(\mathbb{E}_{\mathbf{x}} d_{\text{KL}}(p(y|\mathbf{x})||p(y)))$ , where  $d_{\text{KL}}$  denotes the Kullback-Liebler divergence of two distributions. The distribution  $p(y|\mathbf{x})$  was originally designed to be used with the Inception network [40], but we instead use a pre-trained classifier for the dataset at hand. Notice that this metric does not require any information about the disentangled representation of a sample. Inception score is widely used in the GAN literature to evaluate data quality. We also describe more nuanced measures of image quality in Appendix D, and measure them on our datasets.

Intuitively, inception score measures a combination of two effects: mode collapse and individual sample quality. To tease apart these effects, we compute two additional metrics. The first is *reverse KL-divergence*, proposed in [39] to measure mode collapse in labelled data. It measures the KL-divergence between the generated label distribution and the true distribution. The second is *classifier confidence*, which we use as a proxy for sample quality. Classifier confidence is measured as the argmax of the softmax layer of a pre-trained classifier; the higher this value, the more confident the classifier is in its output, which suggests the image quality is better.

## E dSprites Dataset

### E.1 Parameter Exploration

To better understand the parameter exploration in Figure 4a, we generate similar plots, except representing image quality by mode-reversed KL-divergence (Figure 7) and classifier confidence (Figure 8).

For both reverse KL-divergence and classifier confidence, we observe similar trends to Figure 4a; increasing  $\alpha$  improves disentanglement to a point, whereas it appears to hurt both image quality metrics. One observation is that for  $\alpha \in \{0, 1\}$ , there is little noticeable change in the either image quality metric. This suggests that CR does not introduce mode collapse or substantial reductions in image quality for small  $\alpha$ .

### E.2 Total Correlation

To explore the relation between total correlation and disentanglement, Figure 9 plots the disentanglement score of [23] as a function of dHSIC score while varying  $\alpha$  for InfoGAN-CR. Each point represents a single model, and point size/color signifies the value of  $\alpha \in \{0, 1, 2, 4, 8\}$ . Larger points denote larger  $\alpha$ . Since dHSIC approximates the total correlation between the latent codes, a lower dHSIC score implies a lower total correlation. Perhaps surprisingly, we find a noticeable positive correlation between dHSIC score and disentanglement. This suggests that TC regularization (i.e., encouraging small TC) actually hurts disentanglement for InfoGAN-CR. This may help to explain, or at least confirm, the findings in Figure 4c, which show that adding TC regularization to InfoGAN-CR reduces the disentanglement score.

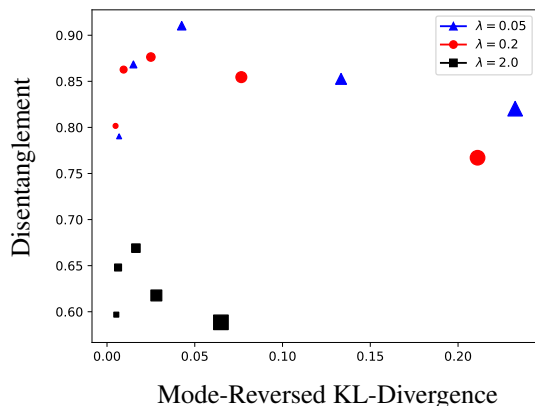


Figure 7: Achievable (mode-reversed KL-divergence, disentanglement) pairs for InfoGAN-CR, where disentanglement is measured as in [23]. We vary the contrastive regularizer  $\alpha$  and the InfoGAN regularizer. The size of each point denotes  $\alpha$ , ranging from smallest to largest for  $\alpha \in \{0, 1, 2, 4, 8\}$ .

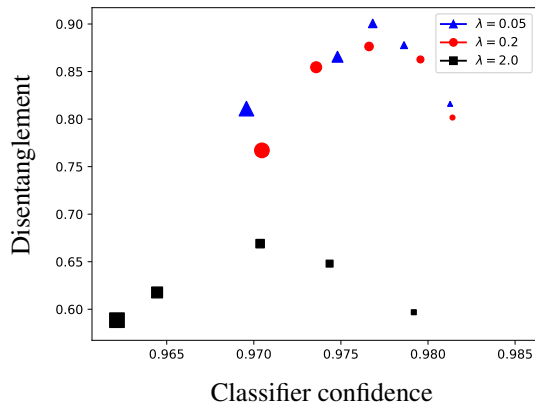


Figure 8: Achievable (classifier confidence, disentanglement) pairs for InfoGAN-CR, where disentanglement is measured as in [23]. We vary the contrastive regularizer  $\alpha$  and the InfoGAN regularizer. The size of each point denotes  $\alpha$ , ranging from smallest to largest for  $\alpha \in \{0, 1, 2, 4, 8\}$ .

### E.3 Contrastive regularizer without InfoGAN regularizer

To test if InfoGAN regularizer is necessary, we trained dSprites dataset without InfoGAN regularizer (i.e.  $\lambda = 0$ ) and progressively increasing  $\alpha$ . This new loss suffers from significant mode collapse, which can be significantly reduced with a recent technique for mitigating mode collapse known as PacGAN introduced in [27]. The main idea is to life the adversarial discriminator to take  $m$  samples packed together, all from either real data or generated data. This provably introduces an implicit inductive bias towards penalizing mode collapse, which is mathematically defined in [27], in terms of binary hypothesis testing and type I and type II errors. The resulting metric are shown in Figure 10, where even with PacGAN we do not get the desired level of disentanglement without InfoGAN regularizer. We believe that InfoGAN and Contrastive regularizers play complementary roles in disentangling GANs.

### E.4 Implementation Details

In dSprites experiments, we used a convolutional neural network for the FactorVAE encoder, InfoGAN discriminator, and CR discriminator, and a deconvolutional neural network for the decoder, and a multi-layer perceptron for total correlation discriminators. We used the Adam optimizer for



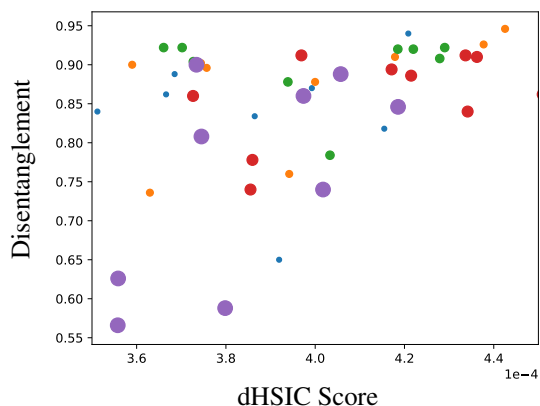


Figure 9: (dHSIC score, disentanglement) pairs for various InfoGAN-CR models. Each point represents a single model, and point size/color signifies the value of  $\alpha \in \{0, 1, 2, 4, 8\}$ . Larger points denote larger  $\alpha$ . Disentanglement is measured as in [23]. We observe a positive correlation between disentanglement and dHSIC score, suggesting that TC regularization does not help GANs disentangle better.

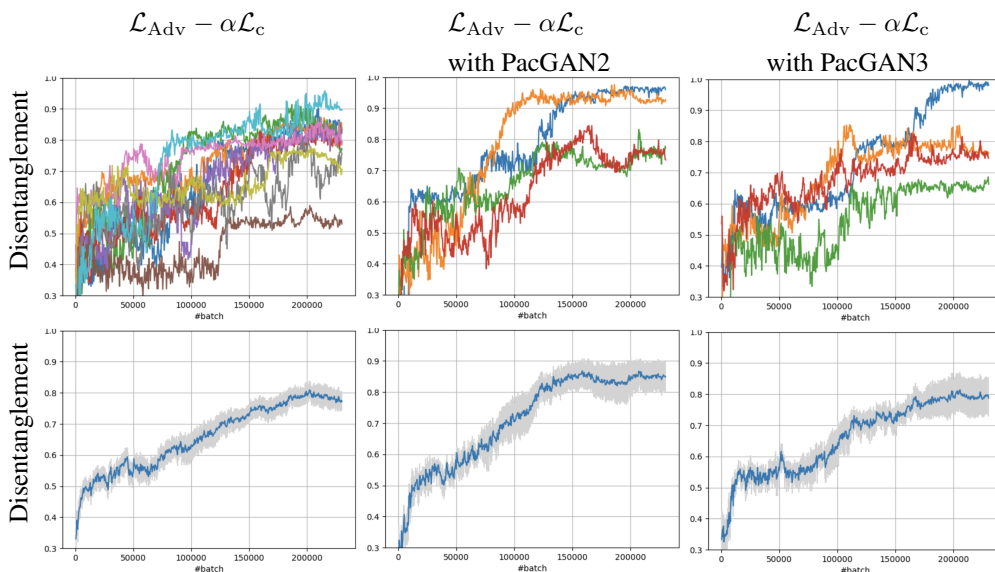


Figure 10: Training without InfoGAN loss suffers from severe mode collapse, which in turn results in poor disentanglement score (left). With PacGAN2 discriminator that takes 2 packed samples together each time, the mode collapse significantly decreases and disentanglement also improves (middle). With PacGAN3 discriminator that takes 3 packed samples together each time, the higher dimensionality of those packed samples results in poor performance (right). The training trajectory of each instance is shown on the top, and the average is shown on the bottom.

all updates, whose learning rates are described below. For unmodified InfoGAN, we used the architecture described in Table 5 of [23]. This architecture is reproduced in Table 3 for completeness. As mentioned in Section 2, we make several changes to the training of InfoGAN to improve its disentanglement, including changing the Adam learning rate to 0.001 for the generator and 0.002 for the InfoGAN and CR discriminators ( $\beta_1$  is still 0.5). The architectural changes are included in Table 4. We include in Table 5 the architecture of our CR discriminator, which is similar to the InfoGAN discriminator. Finally, Table 7 contains the architecture of FactorVAE, reproduced from [23]. We use a batch size of 64 for all experiments.

<b>Discriminator <math>D</math> / Encoder <math>Q</math></b>	<b>Generator <math>G</math></b>
Input $64 \times 64$ binary image	Input $\in \mathbb{R}^{10}$
$4 \times 4$ conv. 32 lReLU. stride 2	FC. 128 ReLU. batchnorm
$4 \times 4$ conv. 32 lReLU. stride 2. batchnorm	FC. $4 \times 4 \times 64$ ReLU. batchnorm
$4 \times 4$ conv. 64 lReLU. stride 2. batchnorm	$4 \times 4$ upconv. 64 lReLU. stride 2. batchnorm
$4 \times 4$ conv. 64 lReLU. stride 2. batchnorm	$4 \times 4$ upconv. 32 lReLU. stride 2. batchnorm
FC. 128 lReLU. batchnorm (*)	$4 \times 4$ upconv. 32 lReLU. stride 2. batchnorm
From *: FC. 1 sigmoid. (output layer for D)	$4 \times 4$ upconv. 1 sigmoid. stride 2
From *: FC. 128 lReLU. batchnorm. FC 5 for $Q$	

Table 3: InfoGAN architecture for dSprites experiments from [23]. We used 5 continuous codes and 5 noise variables.

<b>Discriminator <math>D</math> / Encoder <math>Q</math></b>	<b>Generator <math>G</math></b>
Input $64 \times 64$ binary (dSprites) or color (teapots) image	Input $\in \mathbb{R}^{10}$
$4 \times 4$ conv. 32 lReLU. stride 2. spectral normalization	FC. 128 ReLU. batchnorm
$4 \times 4$ conv. 32 lReLU. stride 2. spectral normalization	FC. $4 \times 4 \times 64$ ReLU. batchnorm
$4 \times 4$ conv. 64 lReLU. stride 2. spectral normalization	$4 \times 4$ upconv. 64 lReLU. stride 2. batchnorm
$4 \times 4$ conv. 64 lReLU. stride 2. spectral normalization	$4 \times 4$ upconv. 32 lReLU. stride 2. batchnorm
FC. 128 lReLU. spectral normalization (*)	$4 \times 4$ upconv. 32 lReLU. stride 2. batchnorm
From *: FC. 1 sigmoid. (output layer for D)	$4 \times 4$ upconv. 1 (dSprites) or 3 (teapots) sigmoid. stride 2
From *: FC. 128 lReLU. spectral normalization	
FC 5. spectral normalization (output layer for $Q$ )	

Table 4: InfoGAN (modified) architecture for dSprites and teapots experiments. We used 5 continuous codes and 5 noise variables.

## F Teapots Dataset

We now discuss implementation details and additional experiments on the teapots dataset. We used an identical architecture to the dSprites dataset for InfoGAN and FactorVAE. For InfoGAN-CR, the CR discriminator architecture changed slightly and is listed in Table 6. As with dSprites, FactorVAE used 10 latent codes, so we chose the best five to compute the disentanglement metric. We also plot the disentanglement metric during training in Appendix F.

For InfoGAN-CR, we train InfoGAN with  $\lambda = 0.2$  for 50000 batches, and then InfoGAN-CR with  $\lambda = 0.2$ ,  $\alpha = 3.0$ , gap=1.9 for 35000 batches, and then InfoGAN-CR with  $\lambda = 0.2$ ,  $\alpha = 3.0$ , gap=0.0 for 40000 batches. We use a batch size of 64 for all experiments. The decoder, disentangling discriminator architectures are the same as dSprites experiments. CR architecture is shown in Table 6.

We illustrate a latent traversal for the teapot dataset under InfoGAN-CR in Figure 12, which is from the best run of InfoGAN-CR with disentanglement metric of [23] 1.0. To make the traversal easier to interpret, we have separated the color channels for each latent factor that captures color. This shows that each latent factor controls a single color channel, while the others are held fixed. A similar traversal is shown in Figure 13 for FactorVAE, which is from the best run of FactorVAE with  $\beta = 40$  and disentanglement metric of [23] 0.94. Although it is difficult to draw conclusions from qualitative comparison, we found that the sharpness of images was reduced in the FactorVAE images, though FactorVAE is able to learn a meaningful disentanglement with three color factors and three (one duplicate) rotation factors.

Building on Table 2, we also plot the disentanglement metric of [23] during the training of InfoGAN-CR and FactorVAE in Figure 11. This plot shows that InfoGAN-CR achieves a consistently higher disentanglement score than FactorVAE throughout the training procedure, though FactorVAE comes close when  $\beta = 40$ .

<b>CR Discriminator</b>
Input $64 \times 64 \times 2$ (2 binary images)
$4 \times 4$ conv. 32 IReLU. stride 2. spectral normalization
$4 \times 4$ conv. 32 IReLU. stride 2. spectral normalization
$4 \times 4$ conv. 64 IReLU. stride 2. spectral normalization
$4 \times 4$ conv. 64 IReLU. stride 2. spectral normalization
FC. 128 IReLU. spectral normalization
FC 5. softmax

Table 5: CR discriminator architecture for dSprites experiments.

<b>CR Discriminator</b>
Input $64 \times 64 \times 6$ (2 color images)
$4 \times 4$ conv. 32 IReLU. stride 2.
$4 \times 4$ conv. 32 IReLU. stride 2. batchnorm
$4 \times 4$ conv. 64 IReLU. stride 2. batchnorm
$4 \times 4$ conv. 64 IReLU. stride 2. batchnorm
FC. 128 IReLU. batchnorm
FC 5. softmax

Table 6: CR discriminator architecture for teapots experiments.

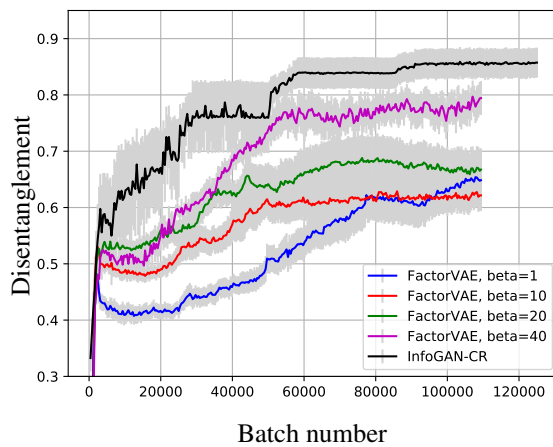


Figure 11: Disentanglement metric of [23] as a function of batch number for InfoGAN-CR and FactorVAE on the teapots dataset. The final models from this training were used to generate Table 2.

Encoder	Decoder
Input $64 \times 64$ binary image	Input $\in \mathbb{R}^{10}$
$4 \times 4$ conv. 32 ReLU. stride 2	FC. 128 ReLU.
$4 \times 4$ conv. 32 ReLU. stride 2.	FC. $4 \times 4 \times 64$ ReLU.
$4 \times 4$ conv. 64 ReLU. stride 2.	$4 \times 4$ upconv. 64 ReLU. stride 2.
$4 \times 4$ conv. 64 ReLU. stride 2.	$4 \times 4$ upconv. 32 ReLU. stride 2.
FC. 128.	$4 \times 4$ upconv. 32 ReLU. stride 2.
FC. $2 \times 10$ .	$4 \times 4$ upconv. 1. stride 2

Table 7: FactorVAE architecture for dSprites and teapots experiments, taken from [23].

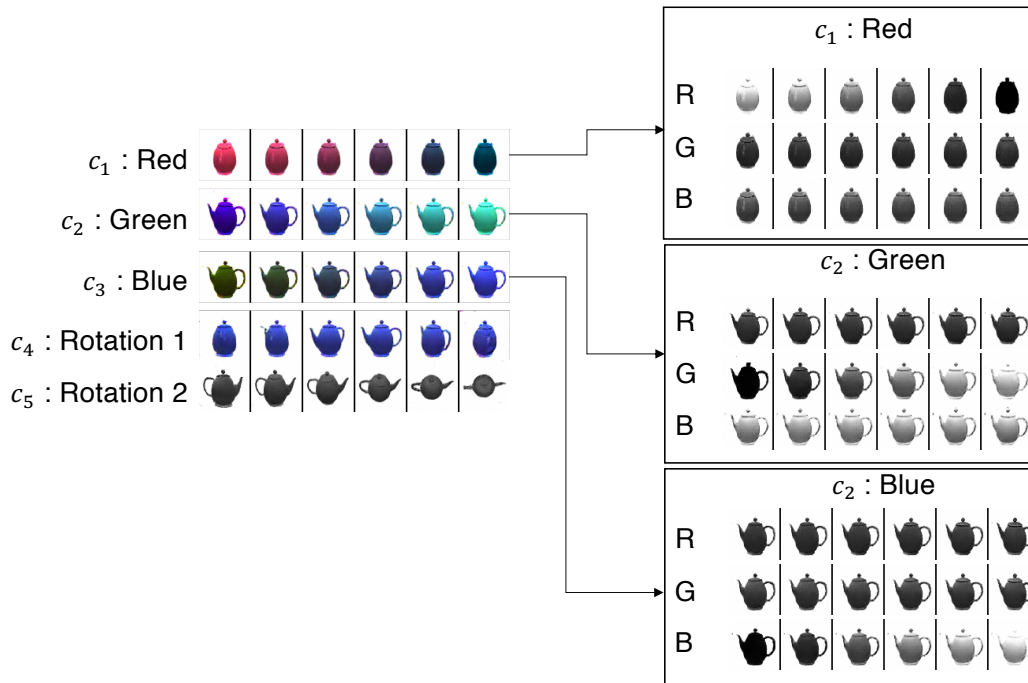


Figure 12: Latent traversal for teapot dataset with InfoGAN-CR. Red (R), blue (B), and green (G) channels are shown separately for the latent factors that correspond to color.

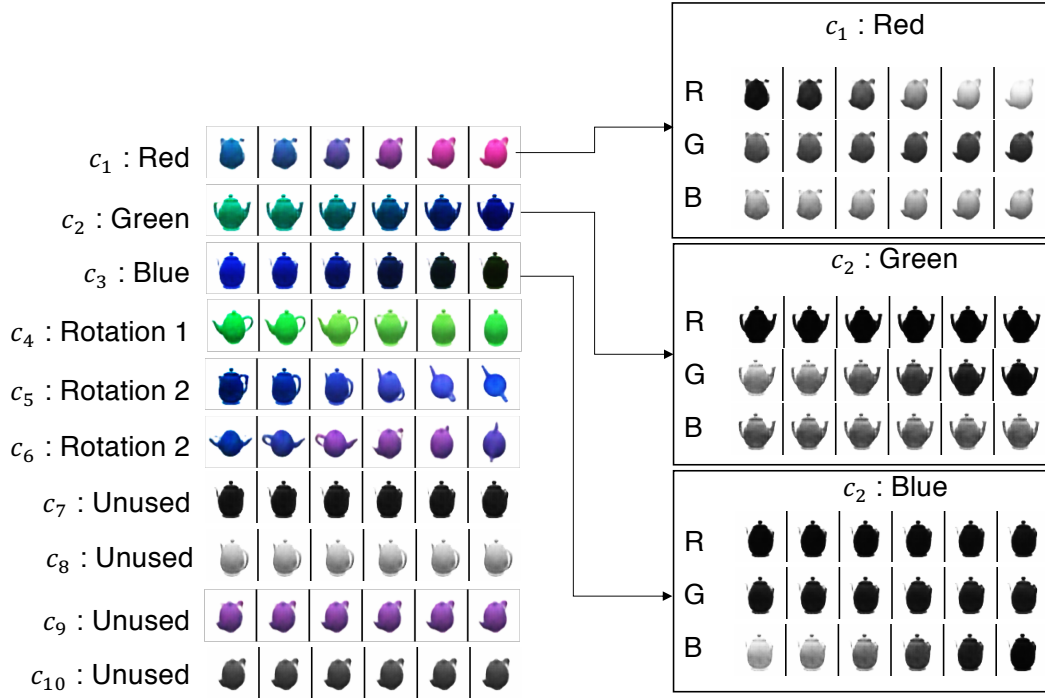


Figure 13: Latent traversal for teapot dataset with FactorVAE. Red (R), blue (B), and green (G) channels are shown separately for the latent factors that correspond to color.

### F.1 Non-commutative and ambiguous coordinate systems

To further push the boundaries of disentangled generation, it is important to understand when and why InfoGAN-CR fails; the teapot dataset gives a useful starting point. In particular, [19] observed that rotations about the canonical basis axes are not commutative. For example, suppose we apply two rotations of some angles, one about the  $x$  and one about the  $y$  axes in two different orders; in general, the resulting orientations of the object need not be the same.

Because of this, a disentangled GAN or VAE trained on a dataset where every possible orientation of teapot is represented should *not* recover the canonical basis for 3D space. Despite this fact, existing experiments (including our own) appear to recover the canonical axes of rotation. To explain this phenomenon, we observe that existing experiments on this dataset, including [12] and our own initial experiments, do not include all orientations of the object in the training data. For example, notice that none of the visualized images in Figure 12 show the bottom of the teapot. Because of the way the training data is selected, the canonical axes are indeed recovered.

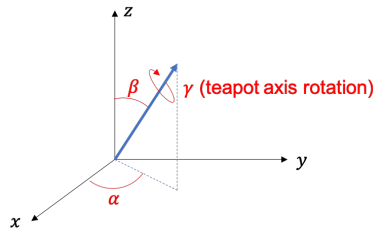


Figure 14: A commutative 3D rotational coordinate system.

We next ask what would happen if all orientations were present in the dataset. To answer this question, first note that in general, 3D rotations can indeed commute. For example, the rotational coordinate system described in Figure 14 commutes. In that coordinate system,  $\gamma$  represents the rotation along

the axis of the teapot (orthogonal to the bottom of the teapot), while  $\alpha$  and  $\beta$  represent the orientation of the teapot’s principal axis. However, this coordinate system is not unique; we could choose a different  $z$ -axis, for instance, and construct a different commutative rotational coordinate system. Hence, even if we were to represent all orientations of the teapots in our training data, it is unclear what orientation we would recover.

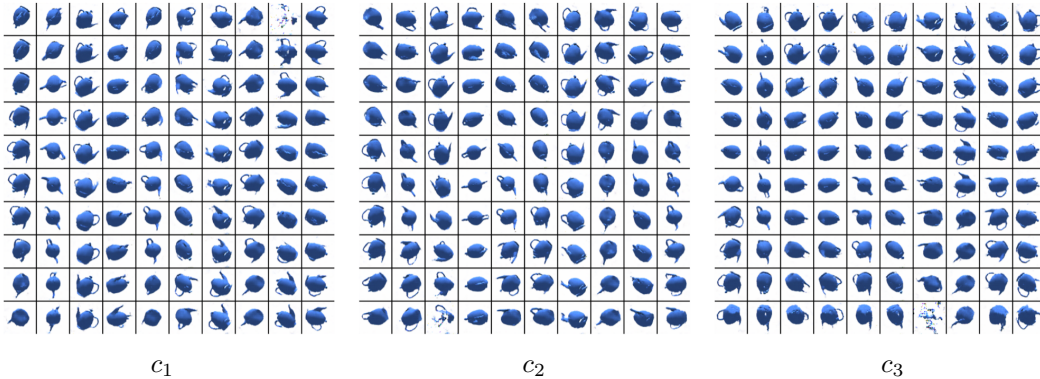


Figure 15: Latent traversal for InfoGAN-CR over the teapot dataset when every possible orientation of the teapot is included. We find that InfoGAN-CR does appear to learn a consistent coordinate axis, even though there is not a unique disentangled representation.

Figure 15 shows the result from a single trial of an experiment where every possible orientation of the teapot is included in the training data. We trained InfoGAN-CR with InfoGAN coefficient  $\lambda = 0.2$  and CR coefficient  $\alpha = 1.0$ . As with our other experiments, we trained five latent factors and visualize the three most meaningful ones in Figure 15. To our surprise, we find that the system (roughly) recovers a similar coordinate system as the one depicted in Figure 14. Here  $c_1$  appears to capture  $\gamma$ ,  $c_2$  appears to recover  $\beta$ , and  $c_3$  recovers  $\alpha$ . Even upon running multiple trials of this experiment, the InfoGAN-CR appears to learn (approximately) the same coordinate system from Figure 14. We hypothesize that this happens because of the illumination in the images. By default, the renderer from [32] renders the teapots with an overhead light source. This may distinguish the vertical axis from the others, causing InfoGAN-CR to learn the vertical axis as a reference for the rotational coordinate system.

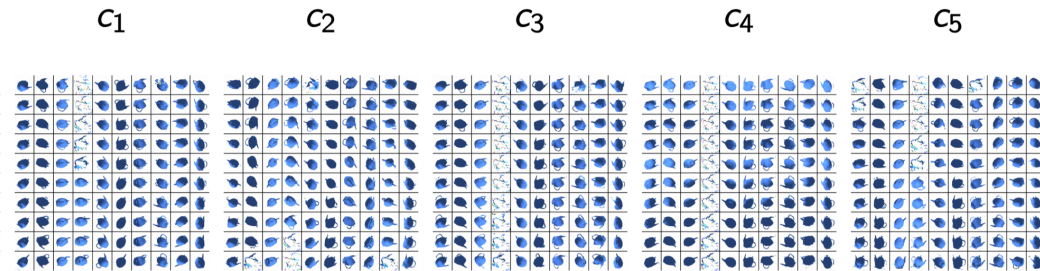


Figure 16: Latent traversal over the teapot dataset when the light source is chosen uniformly for each training image. We find that InfoGAN-CR does not appear to learn a consistent coordinate axis.

To test this hypothesis, Figure 16 shows an experiment in which we randomized the light source for each image. For this experiment, we again used an InfoGAN coefficient of  $\lambda = 0.2$ , and a disentangling coefficient of  $\alpha = 1.0$ ; the experimental setup is identical to that of Figure 15, except for the light source in the training data. We find that in this case, InfoGAN-CR no longer appears to learn the vertical coordinate system. Indeed, it does not seem to learn *any* disentangled representation. We observed similar results for FactorVAE for a range of total correlation coefficients on this dataset, so we do not believe this effect is unique to InfoGAN-CR. Instead, it suggests that in settings where there is no single disentangled representation, current disentanglement methods fail.

## G Circular dSprites (CdSprites) Dataset

To further study the failure modes of our InfoGAN-CR and other state-of-the-art architectures for disentangling, we introduce the following experiments. Towards this purpose we generate a new synthetic dataset which we call Circular dSprites (CdSprites).

It contains a set of 1080,  $64 \times 64$  8-bit gray-scale images generated as follows. Each image has a white (pixel value 255) circular (disc) shape of radius 5 pixels on a black background (pixel value 0). For the placement of the shape we construct a polar (2D) coordinate system, whose co-ordinates are radius  $r \in [0, 32]$  and angle  $\gamma \in [0, 2\pi)$ , and its origin is the center of the image canvas: (32, 32). Then the circular shape is placed on the on a point  $(r, \gamma)$ , such that radius  $r$  is uniformly selected from  $\{0, 1, \dots, 26\}$  (pixel unit) and angle  $\gamma$  is uniformly selected from  $\{0, 2\pi\frac{1}{40}, 2\pi\frac{2}{40}, \dots, 2\pi\frac{39}{40}\}$ . Thus if the center of the circular shape is selected as  $(r, \gamma)$  then it will be placed on the pixel  $(32 + r \cos \gamma, 32 + r \sin \gamma)$ . Thus there are  $27 \times 40$  (1080) total images in the dataset. Fig. 17(a) shows some sample and their corresponding radius ( $r$ ) and angle ( $\gamma$ ) indices. Fig. 17(b) shows the overlap of all the images in the dataset which shows the circular region where the shape can be placed. We expect that a good disentangling representation should disentangle the radius and angle latent factors.

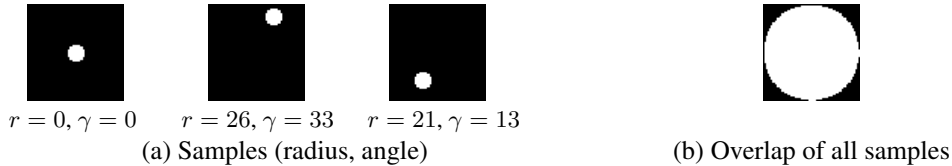


Figure 17: Circular dSprites dataset.

We train FactorVAE, InfoGAN and InfoGAN-CAR models on this dataset. We use the same architecture as the one we use for the dSprites dataset for these models. However, we reduced number of latent factors to 2 for all the models, since there are only two factors to be learned.

In Fig. 18, we show the traversal of the dataset through the true latents. Each row corresponds to one one latent’s traversal while the other is fixed. Each column has a different fixed value for the other fixed latent. As we traverse through a latent keeping the other fixed, for easy visualization, we increase the shade of the shape from the darkest to the brightest. In Figs. 19, 20, and 21, where show the traversal through the learned latents of FactorVAE, InfoGAN, and InfoGAN-CR respectively. We see that the none of the models truly disentangle the true radius and angle factors and in fact they are mixed in the learned learned latents. We believe this dataset is hard for any current models to disentangle, and thus could be used as good baseline for future research.

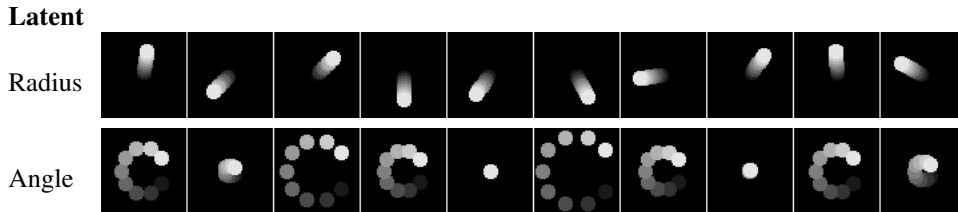


Figure 18: (CdSprites) True latent traversal (see Appendix G for explanation). We see that the top row changes position radially and the bottom row changes the position angularly.

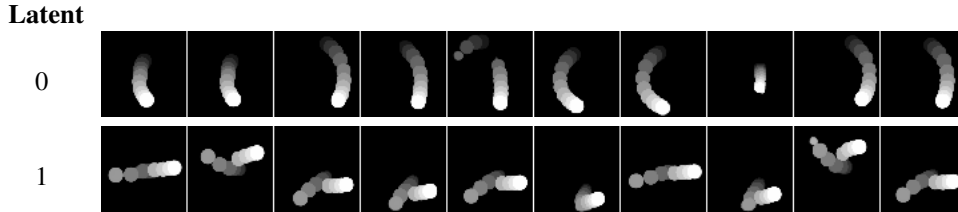


Figure 19: (CdSprites) FactorVAE latent traversal (see Appendix G for explanation). We see that the model does not disentangle the true radius and angle factors and in fact they are mixed.

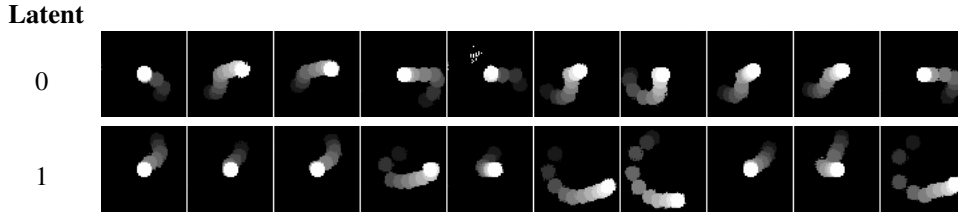


Figure 20: (CdSprites) InfoGAN latent traversal (see Appendix G for explanation). We see that the model does not disentangle the true radius and angle factors and in fact they are mixed.

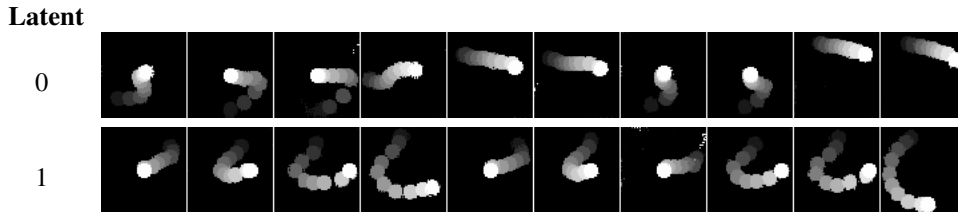


Figure 21: (CdSprites) InfoGAN-CR latent traversal (see Appendix G for explanation). We see that the model does not disentangle the true radius and angle factors and in fact they are mixed.

## H CelebA Dataset

### H.1 Implementation Details

We crop the center  $128 \times 128$  pixels from original CelebA images, and resize the images to  $32 \times 32$  for training.

The architecture of generator, InfoGAN discriminator, CR discriminator in this experiment are shown in Table 8 and Table 9, which are in part motivated by an independent implementation of InfoGAN<sup>8</sup>. We used the Adam optimizer for all updates. Generator’s learning rate is  $2e-3$ , InfoGAN discriminator’s and CR discriminator’s learning rates are  $2e-4$ .  $\beta_1$  is 0.5, batch size is 128 for all components. We train InfoGAN with  $\lambda = 2.0$  for 80000 batches, and then train InfoGAN-CR with  $\lambda = 2.0$ ,  $\alpha = 1.0$ ,  $\text{gap} = 0.0$  for another 10173 batches (so that total number of epoch is 57). The samples are generated from the end of training of one run.

## I Exploring Choices of CR

In the design of CR, there are 4 choices, based on how the two input images are generated, when assuming gap is always zero:

1. Same noise variables, and same latent codes except one
2. Same noise variables, and random latent codes except one

<sup>8</sup><https://github.com/conan7882/tf-gans>



<b>Discriminator <math>D</math> / Encoder <math>Q</math></b>	<b>Generator <math>G</math></b>
Input $32 \times 32$ color image	Input $\in \mathbb{R}^{105}$
$5 \times 5$ conv. 64 lReLU. stride 2. spectral normalization	FC. 1024 ReLU. batchnorm
$5 \times 5$ conv. 128 lReLU. stride 2. spectral normalization	FC. $4 \times 4 \times 256$ ReLU. batchnorm
$5 \times 5$ conv. 256 lReLU. stride 2. spectral normalization	$5 \times 5$ upconv. 128 ReLU. stride 2. batchnorm
$5 \times 5$ conv. 512 lReLU. stride 2. spectral normalization (*)	$5 \times 5$ upconv. 64 ReLU. stride 2. batchnorm
From *: FC. 1 sigmoid. (output layer for D)	$5 \times 5$ upconv. 3 tanh. stride 2
From *: FC. 5. spectral normalization (output layer for $Q$ )	

Table 8: InfoGAN architecture for CelebA experiments. We used 5 continuous codes and 100 noise variables.

<b>CR Discriminator</b>
Input $32 \times 32 \times 6$ (2 color images)
$5 \times 5$ conv. 64 lReLU. stride 2.
$5 \times 5$ conv. 128 lReLU. stride 2. batchnorm
$5 \times 5$ conv. 256 lReLU. stride 2. batchnorm
$5 \times 5$ conv. 512 lReLU. stride 2. batchnorm
FC 5. softmax

Table 9: CR discriminator architecture for CelebA experiments.

3. Random noise variables, and same latent codes except one
4. Random noise variables, and random latent codes except one

We tried all four settings in MNIST dataset, using architecture in [8], with 1 10-category latent codes, 2 continuous latent codes, and 62 noise variables. We had 8 runs for each setting, and visually inspect whether it correctly disentangle digit, rotation, and width. The disentanglement successful rate are recorded in table 10.

Choice	Rate of Successful Disentanglement
1	5/8
2	8/8
3	2/8
4	6/8

Table 10: Rate of successful disentanglement using four choices of CR

Based on this result, we choose to use option 2 as our starting point of designing CR.